Antarct. Meteorite Res., **16**, 34–57, 2003


# Mineralogy and petrology of Yamato 000593: Comparison with other Martian nakhlite meteorites

Takashi Mikouchi, Eisuke Koizumi, Akira Monkawa, Yuji Ueda and Masamichi Miyamoto

*Department of Earth and Planetary Science, Graduate School of Science, University of Tokyo, Hongo 7-chome, Bunkyo-ku, Tokyo 113–0033*

***Abstract:*** Yamato (Y) 000593 is a new nakhlite recovered from Antarctica and is composed of roughly 80% augite, 10% olivine and 10% mesostasis. Augite is chemically homogeneous except for Fe-rich rims adjacent to the mesostasis. Olivine has more extensive chemical zoning, but the most Fe-rich part is also near the mesostasis. These observations suggest that chemical zoning of both augite and olivine was produced by interaction with the mesostasis. The crystallization history of Y000593 as deduced from this study is as follows. (1) Crystallization of cumulus augite and olivine and formation of symplectites in olivine. (2) Accumulation of augite and olivine. (3) Mesostasis crystallization and interaction of the augite and olivine rims with the intercumulus melt. (4) Aqueous alteration. The petrography and mineralogy of Y000593 is generally similar to other nakhlites, but minor mineralogical differences are observed. These differences resulted from different thermal histories due to different locations (burial depths) in the same cooling cumulate pile. Y000593 is most similar to Nakhla and both samples experienced similar formation histories. However, later mesostasis crystallization of Y000593 was more rapid than Nakhla due to its faster cooling rate. The burial depth of Y000593 would be shallower than 3 m from the surface, and is intermediate between NWA817 and Nakhla. The abundance and mineralogy of the mesostasis as well as augite and olivine rim compositions are related to the burial depths of nakhlites.

**key words**: nakhlite, augite, olivine, crystallization, cooling rate

## 1. Introduction

Among more than twenty known samples of Martian meteorites, six samples (Nakhla, Lafayette, Governador Valadares, Northwest Africa 817, Yamato 000593/000749/000802 and Northwest Africa 998) show similar petrography and chemistry, constituting a "nakhlite" group (*e.g.*, Bunch and Reid, 1975; Harvey and McSween, 1992a; Imae *et al.*, 2002a; Irving *et al.*, 2002; McSween, 1994; Meyer, 1998; Sautter *et al.,* 2002). Nakhlites are cumulus clinopyroxenites with minor amounts of olivine and mesostasis. All the known nakhlites show very similar mineralogy, as well as similar crystallization and cosmic-ray exposure ages (1.3 Ga and 10–11 Ma, respectively) (*e.g.*, Bogard *et al.*, 1984; Bogard, 1995; Bunch and Reid, 1975; Eugster *et al.*, 1997; Harvey and McSween, 1992a; Marty *et al.*, 2001; Mikouchi and Miyamoto, 1998, 2002; Nakamura *et al.*, 1982; Reid and Bunch, 1975; Sautter *et al.*, 2002; Shih *et al.*, 1996,

1998; Wadhwa and Crozaz, 1995). However, minor differences in mineralogy have been pointed out among nakhlite samples (*e.g.*, Harvey and McSween, 1992a; Lentz *et al.*, 1999; Mikouchi and Miyamoto, 1998, 2002; Sautter *et al.*, 2002). It is believed that such mineralogical differences, albeit slight, are due to different degrees of late magmatic and subsolidus atomic diffusion due to different locations in the same cooling cumulate pile (*e.g.*, Harvey and McSween, 1992a). Therefore, the discovery of new nakhlite samples could offer substantial information to better understand the formation conditions and geological setting of this unique Martian meteorite group.

Yamato 000593, Yamato 000749, and Yamato 000802, which are possibly paired, are the first samples of nakhlites from Antarctica (Kojima and Imae, 2001; Imae *et al.*, 2002a, b). Yamato 000593 (hereafter, Y000593) is the largest achondrite sample in the Antarctic meteorite collections (Imae *et al.*, 2002c). In this paper, as a part of the consortium study of the Yamato nakhlites (Kojima *et al.*, 2002), we present mineralogy and petrology of Y000593 to understand its formation conditions. We also compare the mineralogy of Y000593 with those of other nakhlites to discuss the mineralogical relationships between Y000593 and other nakhlites.

## 2. Samples and analytical techniques

We studied three polished thin sections of Y000593 (Y000593,62-3, Y000593,62-6, and Y000593,68-1) supplied from the National Institute of Polar Research (NIPR). Back-scattered electron (BSE) images were taken with JEOL JXA840 and Hitachi S-4500 (field emission gun) scanning electron microscopes with energy dispersive spectrometers (EDS), respectively (Dept. of Earth and Planet. Sci., University of Tokyo). X-ray elemental distribution maps were acquired by a JEOL JXA 8900L electron microprobe (Dept. of Earth and Planet. Sci., University of Tokyo). Accelerating voltage was 15 kV, and the beam current was 60–80 nA. Quantitative wavelength dispersive analyses were performed on a JEOL Superprobe 733 electron microprobe (Ocean Research Institute, University of Tokyo) and a JEOL JCM 733 mk II microprobe (Dept. of Earth and Planet. Sci., University of Tokyo) by using natural and synthetic standards. Microprobe analyses of most phases were obtained by focused beam at 15 kV accelerating voltage with a beam current of 12 nA. For feldspar minerals in the mesostasis, a defocused beam of ~5 $\mu$m diameter was employed. The petrography and mineral compositions of Y000593 were compared with those of other nakhlites by using data contained in Mikouchi and Miyamoto (1998) and Mikouchi and Miyamoto (2002) for Nakhla, Governador Valadares and Lafayette and Mikouchi and Miyamoto (2001) for Northwest Africa 817 (hereafter, NWA817). Because we have not analyzed Northwest Africa 998 and its available mineralogical data are limited at present, we do not consider this meteorite in this paper.

## 3. Petrography

All the Y000593 thin sections studied show a similar unbrecciated cumulus texture with the modal abundances of minerals, ~80% augite, 10% olivine, and 10% mesostasis (Fig. 1). We did not observe any obvious differences in modal abundances among the

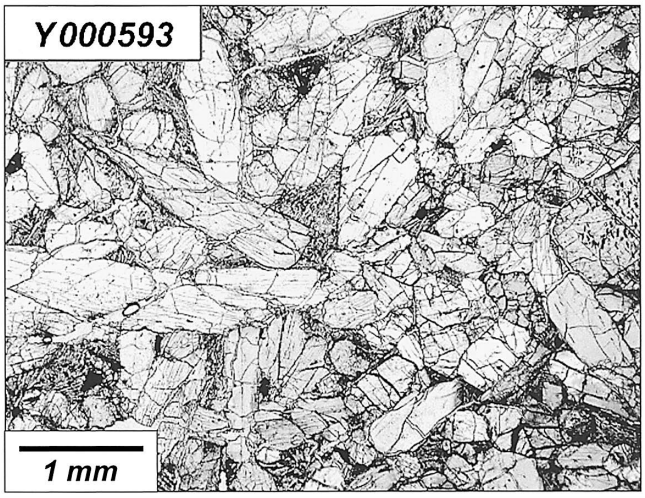


*Fig. 1a. Optical photomicrograph (open nikol) of the Y000593 thin section (Y000593,68-1). The thin section shows a cumulate texture mainly composed of augite, olivine and the mesostasis. Augite shows a prismatic crystal texture up to 1.5 mm long.*

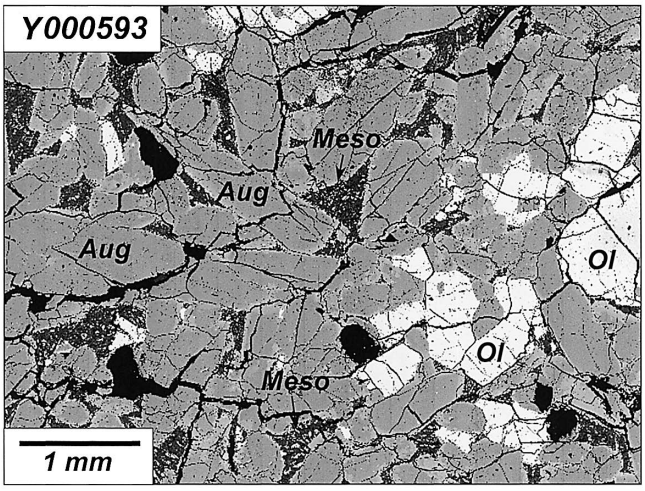


*Fig. 1b. Back-scattered electron (BSE) image of the same field of view as Fig 1a. Bright phases are mostly olivines. Augite is principally homogeneous except for the rims adjacent to the mesostasis. Aug: augite. Ol: olivine. Meso: mesostasis.*

three thin sections.

Augite commonly occurs as euhedral to subhedral elongated grains whose longer dimension reaches up to 1.5 mm (Fig. 1). Polysynthetic twinning is commonly observed. It is likely that augite is a cumulus phase as in other nakhlites, because of its high abundance and a preferred orientation (though not so obvious in our samples) of the longer dimensions of the grains. Minor amounts of low-Ca pyroxene are present (~1 vol%) and are usually associated with the mesostasis.

Olivine grains are mostly anhedral and interstitial to cumulus augite (Fig. 1b). The size of typical olivine grains is similar to that of pyroxene and they sometimes show euhedral crystal termination adjacent to the mesostasis. Small anhedral olivine grains (less than 200 $\mu$m in size) are also found and they are all interstitial to augite. Dark lamellar or patchy inclusions are commonly observed in large olivine grains (Fig. 2a).

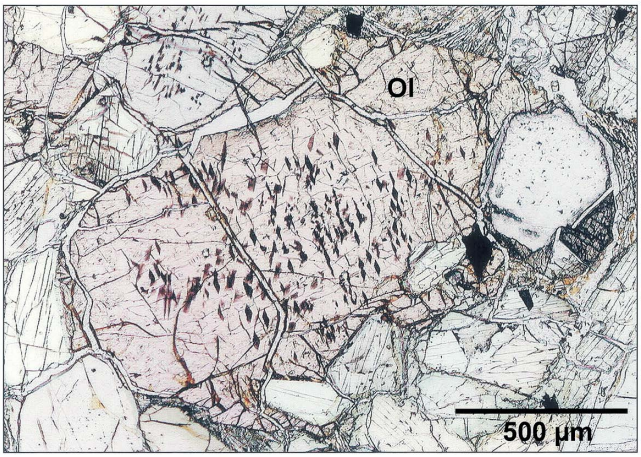


*Fig. 2a. Optical photomicrograph (open nikol) of one of the largest olivine grains in Y000593. The presence of dark lamellar (or rectangular in this image) inclusions throughout the crystal is remarkable. Brown alteration products are observed around the rim and the fractures. Ol: olivine.*

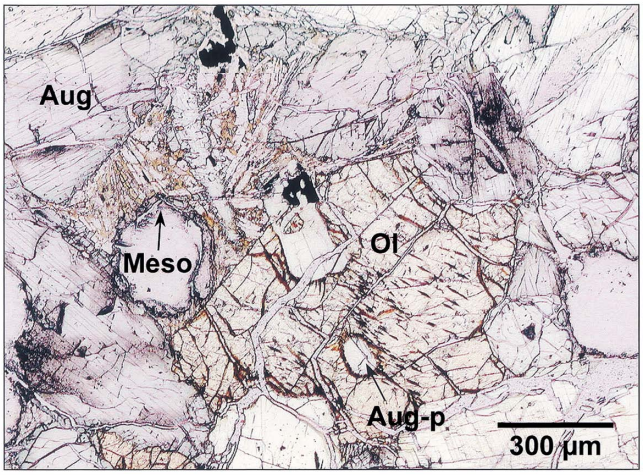


*Fig. 2b. Optical photomicrograph (open nikol) of an altered olivine grain in Y000593. The presence of brown alteration products along the fractures is remarkable in this olivine grain. This olivine grain contains a poikilitic augite grain (Aug-p). The mesostasis (Meso) is also showing alteration similar to olivine. Ol: olivine. Aug: augite.*

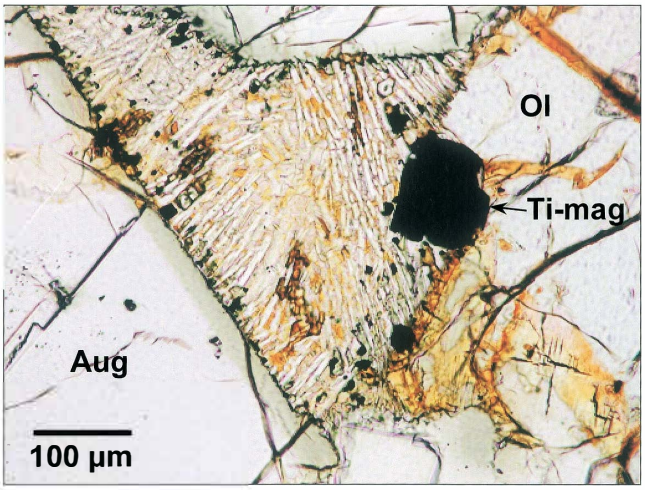


*Fig. 2c Optical photomicrograph (open nikol) of the mesostasis area in Y000593. Note the presence of brown alteration products interstitial to plagioclase laths. The mesostasis includes a Ti-rich magnetite grain (Ti-mag). Some of the tiny opaque grains in the mesostasis are Fe sulfide. Aug: augite. Ol: olivine.*

The distributions of these lamellar inclusions within olivine grains are irregular unlike regular exsolution lamellae. Some large olivine grains poikilitically enclose rounded augite grains whose composition is identical to cumulus augite (Fig. 2b). Although magmatic inclusions are uncommon in olivine grains, single crystal augite inclusions, similar to those reported in Harvey and McSween (1992b), are observed in some olivine grains. These inclusions are rounded with sizes up to 200 $\mu$m and are sometimes associated with K-feldspar. Olivine grains are pervasively altered to brown-colored, fine-grained materials (smectite?) along fractures (Fig. 2b) as reported in Imae *et al.* (2002b) and Treiman and Goodrich (2002).

The mesostasis commonly displays a plumose texture, which is composed predominantly of narrow laths of plagioclase with subordinate proportions of K-rich feldspar and a silica mineral (Fig. 2c). Plagioclase length reaches up to 200–300 $\mu$m although the width is only ~20 $\mu$m. Scattered lath-shaped grains of olivine and augite are also observed within the mesostasis and they are sometimes intergrown with plagioclase (Fig. 2c). Other minor phases in the mesostasis include Ti-rich magnetite (ulvöspinel), ilmenite, Ca phosphate and Fe sulfide (pyrite?). Ti-rich magnetite is up to 300 $\mu$m in size although some grains are not associated with the mesostasis. The mesostasis also shows extensive secondary alteration indicated by the presence of brown rusty products as is seen in olivine (Imae *et al.*, 2002b; Treiman and Goodrich, 2002) (Fig. 2c).

Shock effects appear minor (or moderate) by judging optical and petrological properties of augite and olivine (*e.g.*, slight undulating extinction of augite and olivine, polysynthetic twinning of augite).

## 4. Mineral compositions

Representative mineral compositions of Y000593 are given in Table 1.

### *4.1. Augite*

Most pyroxenes in Y000593 are augite, having a large homogeneous core (average of 153 analyses: $En_{39}Fs_{22}Wo_{39}$. Standard deviations for the En, Fs and Wo components are about 1, respectively) (Figs. 1b and 3). The core composition is identical to that reported in Imae *et al.* (2002a, b). The rims adjacent to the mesostasis show enrichment of Fe (Fig. 1b), but the Wo content is almost uniform ($En_{39}Fs_{22}Wo_{39}$~ $En_{20}Fs_{40}Wo_{40}$) except for the 10–20 $\mu$m edge ($En_{20}Fs_{40}Wo_{40}$~ $En_{15}Fs_{70}Wo_{15}$) (Fig. 3). There is a sharp compositional boundary between the homogeneous core and the Fe-enriched rim as is clear from the high contrast BSE and Fe X-ray images (Figs. 4a and 5). At the boundary with the mesostasis, Fe-rich pyroxene displays a finger-like "overgrowth" texture (or crystallites that have nucleated on the pyroxene) intruding into the mesostasis and similar compositional pyroxene is observed within the mesostasis (Fig. 4b). High-resolution BSE images show the presence of fine exsolution lamellae ($<$500 nm wide) at the 10–20 $\mu$m edges of cumulus pyroxenes adjacent to the mesostasis like other nakhlite pyroxenes (Mikouchi and Miyamoto, 1998) (Fig. 4c). The presence of fine exsolution lamellae is consistent with variable Wo content of pyroxene with constant En content (En: ~15) at the rims (Fig. 3). Similar fine exsolution lamellae are also

*Table 1. Representative mineral compositions of major phases in Y000593.*

| | Augite (Core) | Augite (Rim) | Pigeonite (Fe-rich) | Pigeonite | Olivine (Core) | Olivine (Rim) | Plagioclase | K-feldspar | Ti-magnetite | Ilmenite | Apatite | "Rust" |
|---|---|---|---|---|---|---|---|---|---|---|---|---|
| $SiO_2$ | 52.2 | 49.1 | 47.6 | 48.9 | 34.2 | 32.0 | 59.6 | 66.2 | 0.12 | n.d. | 0.65 | 43.6 |
| $Al_2O_3$ | 0.60 | 1.93 | 0.74 | 0.10 | n.d. | 0.03 | 24.2 | 18.5 | 1.52 | 0.02 | 0.06 | 2.10 |
| $TiO_2$ | 0.18 | 0.48 | 0.35 | 0.05 | n.d. | 0.06 | 0.06 | n.d. | 15.3 | 49.1 | n.d. | 0.02 |
| FeO | 13.0 | 22.2 | 38.1 | 35.8 | 45.5 | 60.1 | 0.85 | 0.45 | 77.0 | 45.6 | 0.49 | 26.9 |
| MnO | 0.39 | 0.57 | 0.92 | 1.01 | 0.92 | 1.15 | 0.06 | n.d. | 0.38 | 0.66 | 0.12 | 0.46 |
| MgO | 13.6 | 7.04 | 3.96 | 9.49 | 18.6 | 6.42 | 0.02 | n.d. | 0.29 | 0.53 | 0.04 | 8.57 |
| CaO | 18.5 | 18.2 | 7.36 | 3.06 | 0.50 | 0.15 | 7.18 | 0.64 | 0.08 | n.d. | 53.5 | 1.60 |
| $Na_2O$ | 0.15 | 0.28 | 0.13 | 0.04 | n.d. | n.d. | 7.56 | 3.92 | n.d. | n.d. | n.d. | 0.25 |
| $K_2O$ | 0.02 | n.d. | n.d. | n.d. | n.d. | n.d. | 0.58 | 9.61 | n.d. | n.d. | 0.03 | 0.43 |
| $Cr_2O_3$ | 0.41 | 0.05 | n.d. | 0.02 | n.d. | n.d. | n.d. | n.d. | 0.07 | 0.09 | 0.07 | n.d. |
| $V_2O_3$ | 0.07 | 0.02 | n.d. | 0.03 | n.d. | n.d. | n.d. | n.d. | 0.29 | 0.22 | n.d. | n.d. |
| NiO | n.d. | 0.02 | n.d. | n.d. | 0.04 | 0.02 | 0.04 | 0.06 | 0.03 | n.d. | n.d. | n.d. |
| $P_2O_5$ | 0.18 | 0.18 | n.d. | 0.06 | n.d. | n.d. | 0.03 | n.d. | 0.03 | n.d. | 41.5 | n.d. |
| Total | 99.3 | 100.1 | 99.1 | 98.6 | 99.8 | 99.9 | 100.2 | 99.3 | 95.2 | 96.2 | 96.5 | 83.9 |
| Fs | 21.4 | 38.2 | 69.8 | 63.2 | | | | | | | | |
| En | 39.7 | 21.6 | 12.9 | 29.9 | | | | | | | | |
| Wo | 38.9 | 40.2 | 17.3 | 6.9 | | | | | | | | |
| Fe#* | 0.351 | 0.639 | 0.844 | 0.679 | 0.578 | 0.840 | | | | | | |
| An | | | | | | | 33.3 | 3.3 | | | | |
| Ab | | | | | | | 63.5 | 37.0 | | | | |
| Or | | | | | | | 3.2 | 59.7 | | | | |

**Fe# = Atomic Fe/(Fe+Mg). n.d. = not determined.*

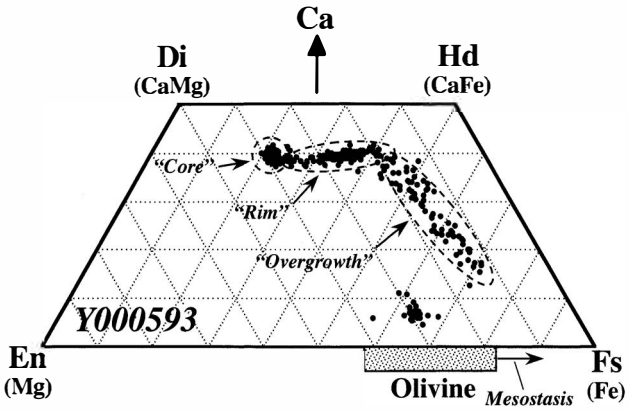


*Fig. 3. Pyroxene quadrilateral of Y000593 with olivine composition (dotted box along the Mg-Fe line). Pyroxene in Y000593 is mainly augite with homogeneous composition (circled as "core"). The rims adjacent to the mesostasis shows Fe-enrichment (circled as "rim"). The extreme edges in contact with the mesostasis have very Fe-rich compositions with variable Wo content due to the presence of fine exsolution (circled as "overgrowth"). Olivine composition has a wide range. The dotted box shows the compositional range observed in cumulus olivine grains. The arrow, "mesostasis", shows more Fe-rich olivine compositions found in the mesostasis.*

observed in small pyroxene grains within the mesostasis (Fig. 4d). The $Al_2O_3$ content of augite ranges 0.4–0.9 wt% (average of 153 analyses: 0.65 wt%. Standard deviation is 0.17) in the core (Fig. 6), showing heterogeneous distribution that is unrelated to the major element composition. The $Al_2O_3$ content increases to 2.0–2.5 wt% towards the rim as atomic Fe/(Fe+Mg) (*fe#*) increases from 0.35 to 0.7 (Fig. 6). The $Al_2O_3$ content suddenly drops down to 0.6–1.0 wt% at the extreme edge (overgrowth) near the mesostasis (Fig. 6). The $TiO_2$ content exhibits a similar behavior, that is, $TiO_2$ is 0.1–0.3 wt% in the core (average of 153 analyses: 0.21 wt%. Standard deviation is 0.06) and shows slight enrichment ($TiO_2$=0.5 wt%) at the rim of *fe#*=0.7 (Fig. 6). At the extreme edge (overgrowth) near the mesostasis, the $TiO_2$ content is 0.3–0.4 wt% (Fig. 6). In contrast to Al and Ti, showing kink compositional trends, the $Cr_2O_3$ content shows monotonous decrease from the core to the rim. In the core, the $Cr_2O_3$ content is 0.3–0.5 wt% (average of 153 analyses: 0.31 wt%. Standard deviation is 0.06) and drops down to nearly 0 at the rim of *fe#*$>$0.6.

Minor amounts of low-Ca pyroxene (pigeonite) are also present as small grains (~200 $\mu$m) usually associated with the mesostasis. It is uniform in composition ($En_{30}Fs_{64}Wo_6$) with $Al_2O_3$ and $TiO_2$ contents that are both less than 0.1 wt%.

### *4.2. Olivine*

Large olivine grains show extensive chemical zoning unlike pyroxenes (Figs. 5 and 7). The most magnesian olivine in the sections studied is $Fa_{58}$ (Fig. 3), which is found near the centers of large olivine grains (Fig. 5). The zoned olivine grains have a very Fe-rich composition of $Fa_{\sim 85}$ at the edges adjacent to the mesostasis, while the rim

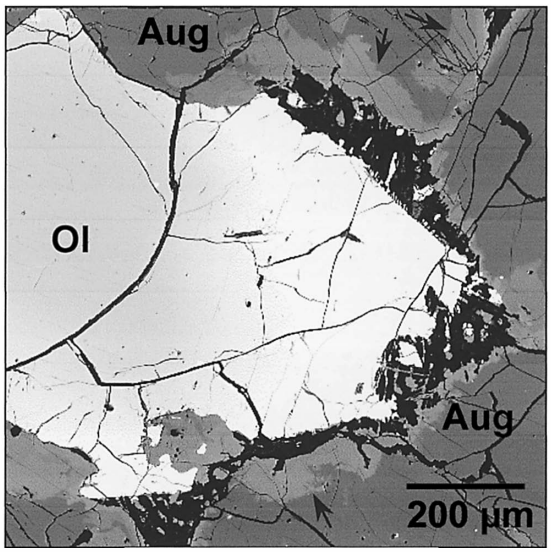


*Fig. 4a. High contrast BSE image of olivine and augite grains in contact with the mesostasis in Y000593. Augite shows sharp compositional boundaries (shown by arrows) between the inner portions and the outer rim portions adjacent to the mesostasis. The olivine grain adjacent to the mesostasis has a well developed crystal termination. Aug: augite. Ol: olivine.*

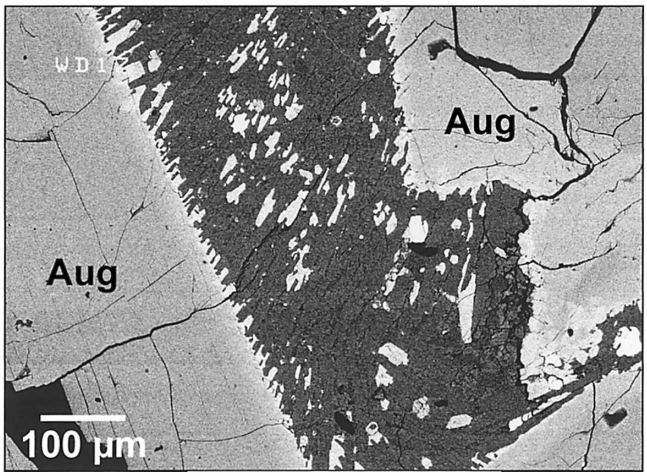


*Fig. 4b. BSE image of augite grains in contact with the mesostasis in Y000593. Augite grains show finger-like textures intruding into the mesostasis at their edges. Pyroxene grains with similar compositions are observed within the mesostasis. Aug: augite.*

compositions adjacent to cumulus augite are less Fe-rich (Fig. 7). Imae *et al.* (2002a, b) also reported similar olivine compositions for Y000593 and Y000749. The most ferroan composition of small olivine grains in the mesostasis reaches $Fa_{91}$. Chemical zoning is more remarkable in larger grains, and small grains (less than ~200 $\mu$m) are

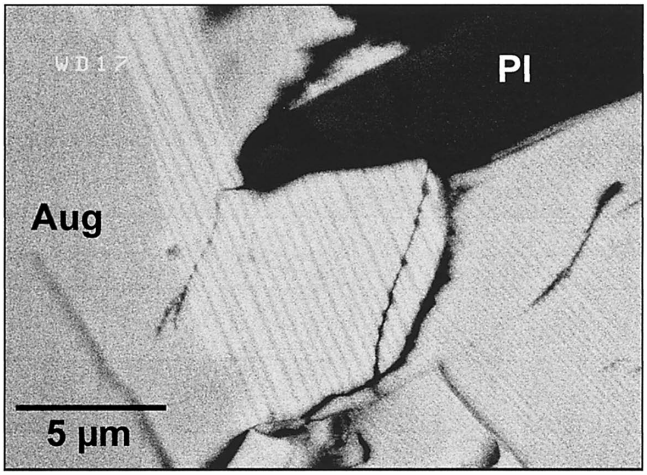


*Fig. 4c. High resolution BSE image of Fe-rich pyroxenes at the cumulus pyroxene rims. Fine exsolution texture (thinner than 500 μm wide) is clearly observed. Probably, darker lamellae correspond to Ca-rich pyroxene and brighter ones are Ca-poor pyroxene. Aug: augite. Pl: plagioclase in the mesostasis.*

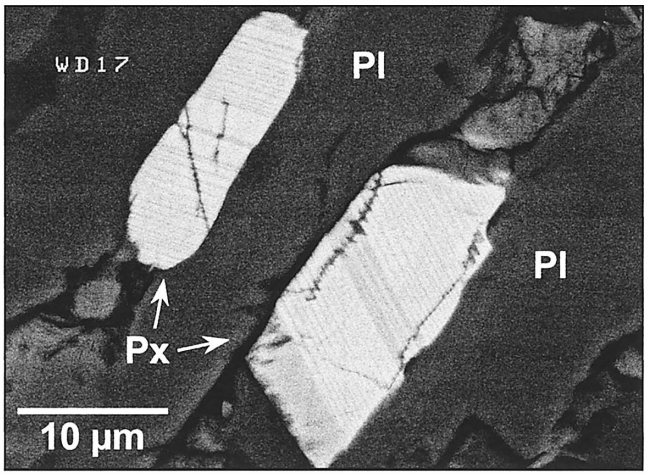


*Fig. 4d. High resolution BSE image of Fe-rich pyroxenes in the mesostasis. These two pyroxene grains also show the presence of fine exsolution lamellae of similar size to that at the pyroxene edges (Fig. 4c). Px: Fe-rich pyroxene in the mesostasis. Pl: plagioclase in the mesostasis.*

usually homogeneous (Fig. 5). The olivine rim composition is similar to those of small grains with homogeneous composition. These observations suggest that chemical zoning can be attributed to cation exchange with the Fe-rich mesostasis. In some cases, olivine grains are intergrown with the mesostasis plagioclase. The CaO content of

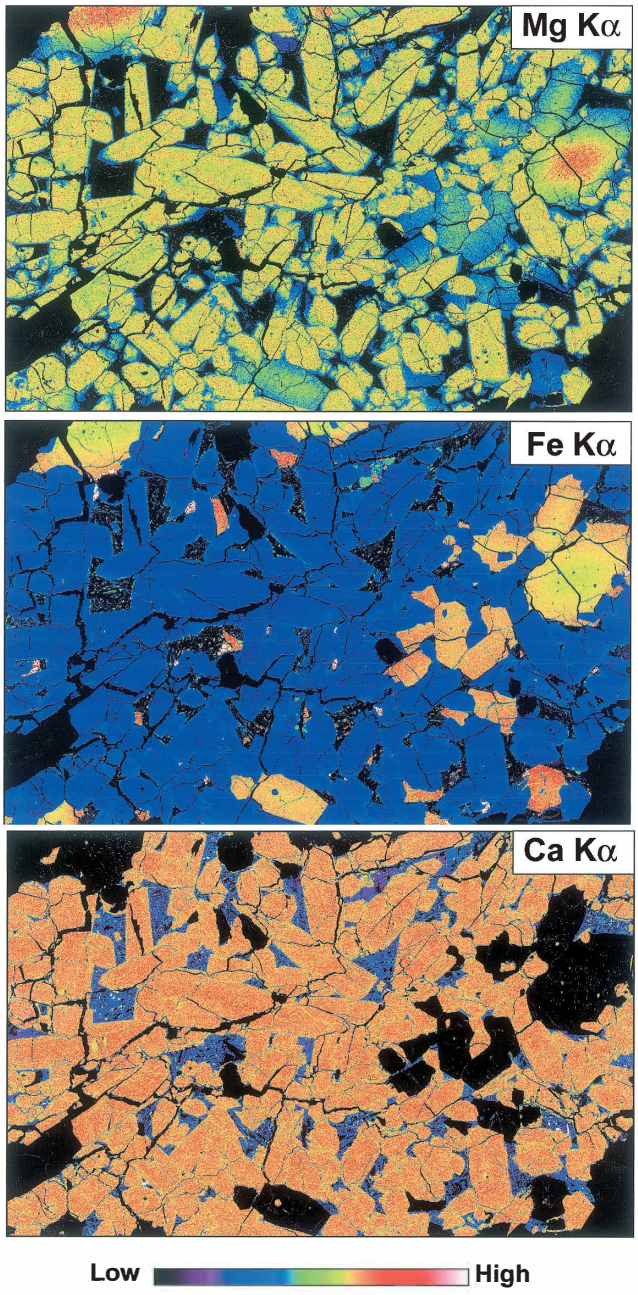


*Fig. 5. Mg, Fe, and Ca X-ray maps of Y000593. The field of view is 9 mm, yielding a slightly larger area than Fig. 1. Yellow grains in the Mg map are cumulus augite. Olivine grains are colored from red to blue due to the presence of chemical zoning. The Fe map also indicates the presence of chemical zoning in olivine (grains showing the green cores to the red rims). Also note the presence of small Fe-rich homogeneous olivine grains. Augite grains (blue) show enrichment of Fe at the rims (core: dark blue, rim: bright blue). The Ca map shows that augite grains have almost uniform Ca content throughout the grains. The color of the mesostasis areas is mostly blue due to the presence of feldspar minerals.*

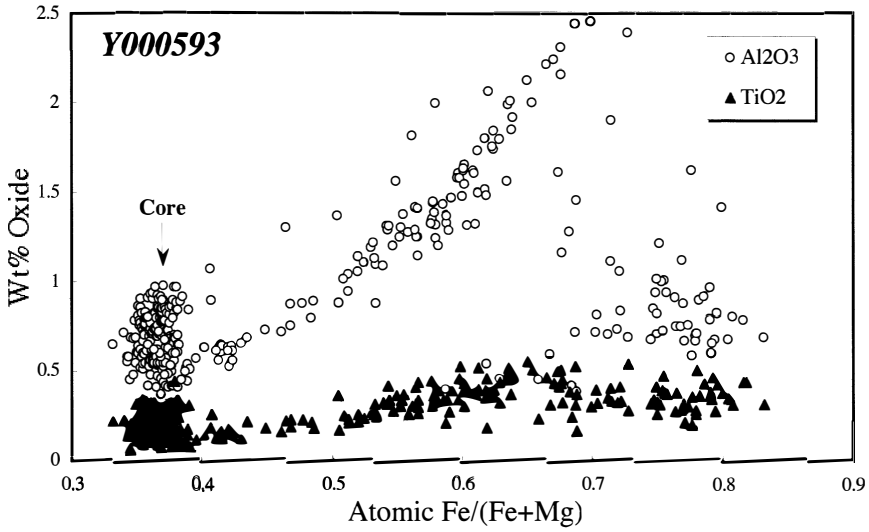


*Fig. 6. Al and Ti variations of augites in Y000593 versus the fe# variation. Al shows the compositional range of $Al_2O_3$=0.4–1.0 wt% in the core, and then increases as fe# increases. The most Fe-rich augite has lower Al contents ($Al_2O_3$=0.5–1.0 wt%). The Ti content also has a cluster in the core ($TiO_2$=0.1–0.3 wt%) and then shows a similar behavior to Al. Ti increases as fe# increase, but it slightly decreases when fe# reaches 0.65.*

olivine is ~0.5 wt% at the core and drops down to 0.1–0.2 wt% at the rim (Fig. 7).

Brownish alteration products present along the olivine fractures (Fig. 2b) have low analytical totals (~85 wt%) (Table 1) and are generally similar to "iddingsite" in other nakhlites (*e.g.*, Imae *et al.*, 2002b; Treiman *et al.*, 1993; Treiman and Goodrich, 2002). They are Mg-poor and relatively enriched in Fe. The low analytical totals suggest the presence of water and ferric iron. However, they have variable compositions, and accurate chemical analysis was almost impossible.

Symplectic inclusions are commonly observed in large olivine grains (Fig. 2a). They are usually parallel to one direction and 50 $\mu$m long and less than 5 $\mu$m thick, but patchy inclusions are also observed (Figs. 8a and 8b). The EDS analysis by FE-SEM suggests that they consist of magnetite (Ti-free) and augite like symplectites in Nakhla and Governador Valadares (Mikouchi *et al.*, 2000). Similar symplectites are also observed at the grain boundaries of cumulus augite as patches ~10 $\mu$m in size (Fig. 8c). Augite inclusions within poikilitic olivine grains are also surrounded by these patches (Fig. 8d).

### *4.3. Mesostasis*

The most abundant phase in the mesostasis is plagioclase, which is usually intergrown with silica or K-feldspar (glass?) (Figs. 2c and 9). The plagioclase composition is $An_{35}Ab_{62}Or_3$~$An_{20}Ab_{74}Or_6$ (Fig. 10) similar to that reported in Imae *et al.* (2002a) and (2002b). These plagioclase grains show clear birefringence under the optical microscope, suggesting that they have not transformed into "maskelynite" by shock. K-feldspar has a wide range of composition and the most K-rich feldspar has an

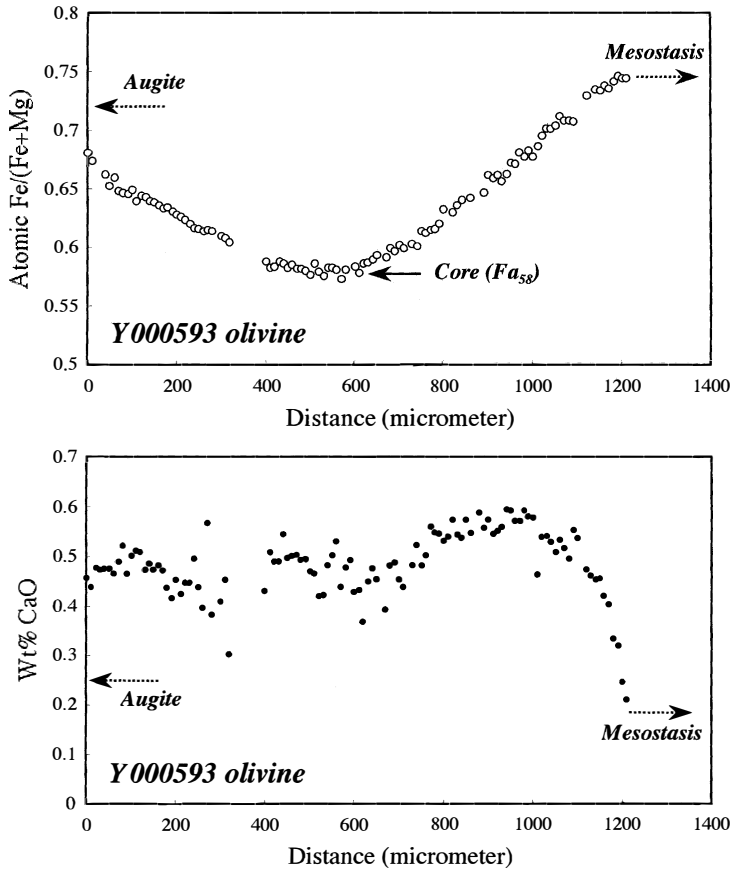


*Fig. 7. The chemical zoning profiles of the atomic Fe/(Fe+Mg) content (Fa content) and Ca content of olivine in Y000593. The dotted arrows show where the olivine grain is in contact with augite and the mesostasis. It is obvious that the rim adjacent to the mesostasis shows more developed zoning patterns in both Fa and Ca. This olivine grain has a core composition of $Fa_{58}$. The Ca zoning is observed at the rim (the area of 1000–1200 μm) whereas Fa zoning penetrates further into the grain (the area of 600–1200 μm). This could be due to different atomic diffusion rates between Fe-Mg and Ca (e.g., Misener, 1974; Jurewicz and Watson, 1988).*

orthoclase content of $Or_{75}$ (Fig. 10). The optical microscopic analysis shows the presence of abundant rusty brown alteration products in the mesostasis as is seen in olivine grains (Fig. 2c). The chemical composition is generally similar to that in olivine. Ca phosphate in the mesostasis is Cl-apatite as the EDS analysis shows the presence of abundant Cl.

### *4.4. Opaques*

Most opaque phases are present within or associated with the mesostasis and/or olivine. Ti-rich magnetite (ulvöspinel) is the most common opaque phase in Y000593. It has a slight variation in chemical composition, ranging 1–3 wt% $Al_2O_3$, 13–18 wt%

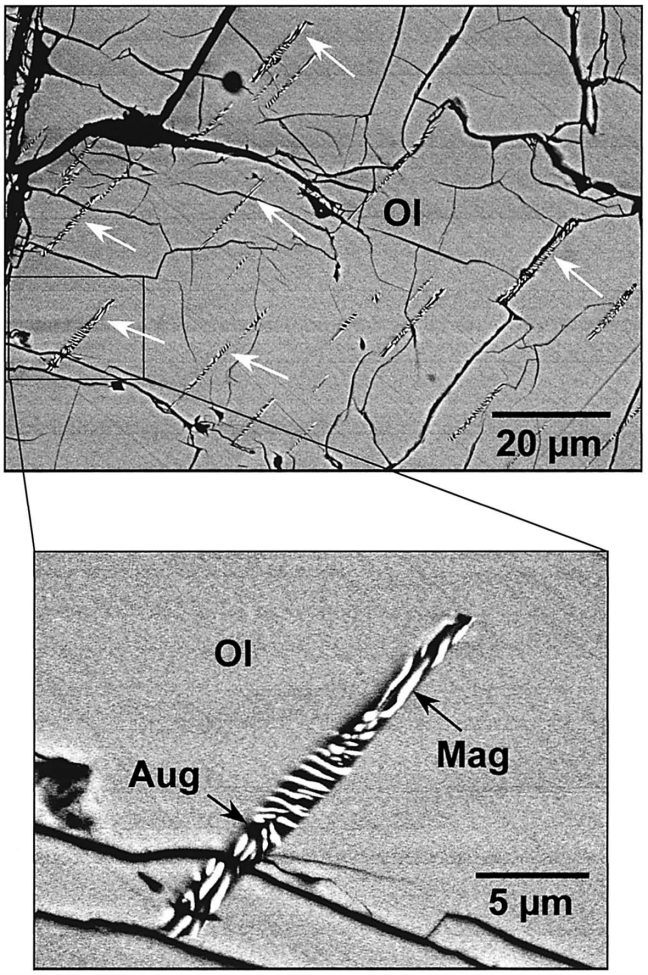


*Fig. 8a. BSE images of an olivine grain in Y000593 including abundant symplectic inclusions (indicated white arrows in the above image). These symplectic inclusions are composed of augite (dark area) and magnetite (bright area). Ol: olivine. Aug: augite. Mag: magnetite.*

$TiO_2$, and 71–77 wt% FeO (all Fe is calculated as $Fe^{2+}$) (Fig. 11). Because the analytical totals are 93–96 wt% (Table 1), significant amounts of $Fe^{3+}$ are probably present. Some Ti-rich magnetite grains include exsolution lamellae of ilmenite up to 5 $\mu$m wide (Fig. 12). Isolated grains of ilmenite were also observed. Fe sulfides are mostly S-rich, probably pyrite rather than pyrrhotite.

## 5. Crystallization history of Y000593

There is no doubt that Y000593 is a cumulate rock like other nakhlites (*e.g.*, Harvey and McSween, 1992a; Wadhwa and Crozaz, 1995; Lentz *et al.*, 1999). Augite is clearly a cumulus phase, but it is not obvious whether olivine is cumulus or not. However, the interaction with the mesostasis is seen in both augite and olivine, causing Fe enrichment at their edges adjacent to the mesostasis. Thus, we believe that olivine is also a cumulus

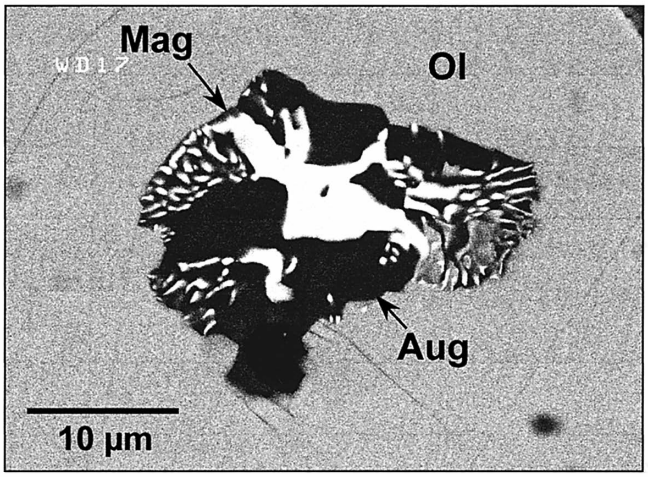


*Fig. 8b. BSE image of the irregularly-shaped patch showing a symplectic texture in a Y000593 olivine grain. This patch is also composed of augite (dark area) and magnetite (bright area). Ol: olivine. Aug: augite. Mag: magnetite.*

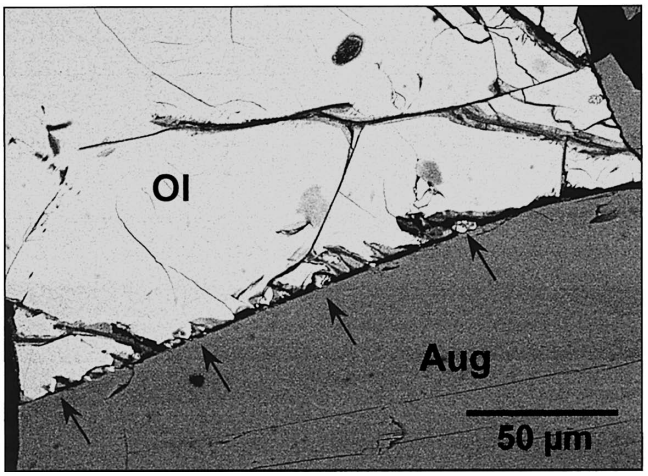


*Fig. 8c. BSE image showing the boundary between cumulus augite (Aug) and olivine (Ol) in Y000593. The arrows show the presence of patches having the symplectic textures similar to Figs. 8a and 8b.*

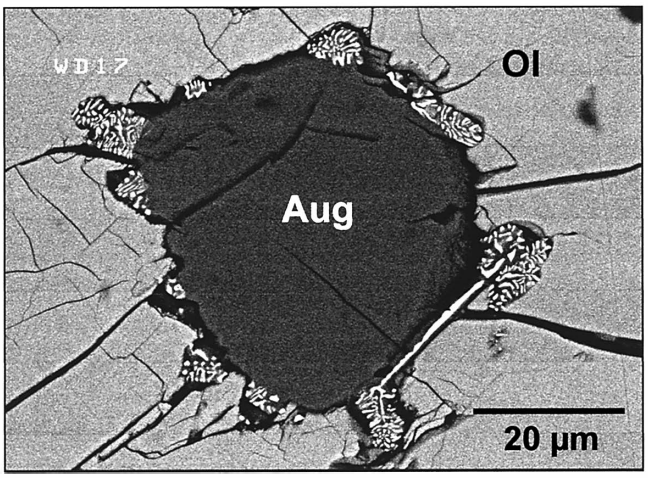


*Fig. 8d. BSE image showing the patches with symplectic textures along the grain boundaries between poikilitic augite (Aug) and the host olivine grain (Ol) in Y000593.*

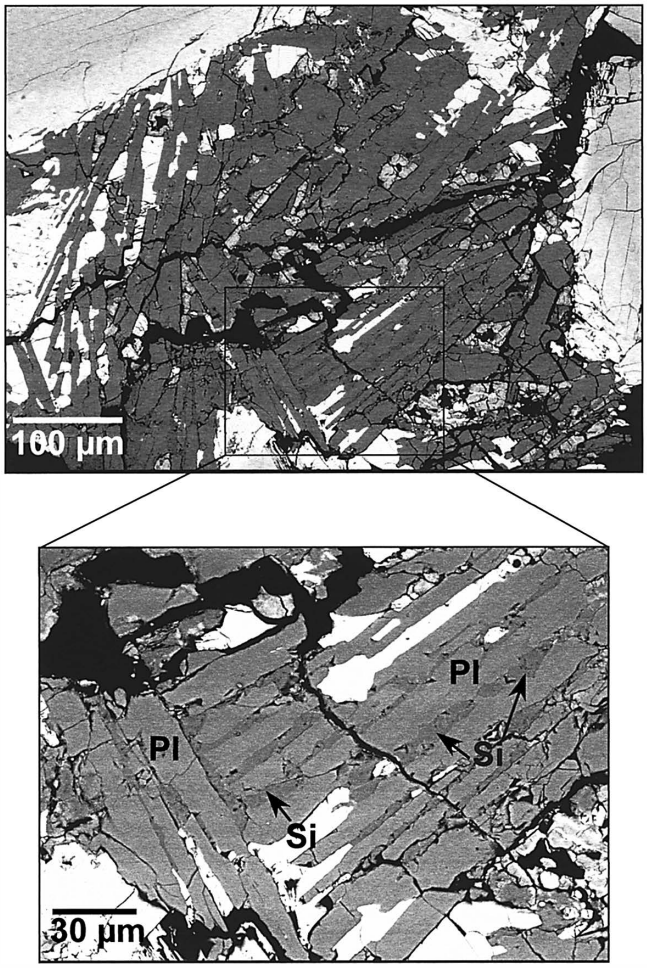


*Fig. 9. BSE images of the mesostasis area in Y000593. The mesostasis is mainly composed of lath-shaped plagioclase (Pl) intergrown with silica (Si). Bright lath-shaped grains in the mesostasis are olivine and pyroxene.*

phase, although its crystallization followed augite crystallization because of the interstitial texture of olivine to augite. However, there is a possibility that olivine cores have nucleated concurrently with the pyroxene and then continued growing (or renewed growth) once pyroxene ceased and accumulation occurred. According to those textural observations, the sequence of the Y000593 crystallization is thus augite, olivine, and the mesostasis. More detailed crystallization history of Y000593 is as follows (Fig. 13).

At first augite crystallized from a magma and olivine crystallization followed. Both augite and olivine show chemical zoning in Y000593. However, augite has a large homogeneous core and the chemical zoning is only seen in the rim area. In contrast, chemical zoning of olivine is much more extensive. This can be explained by faster

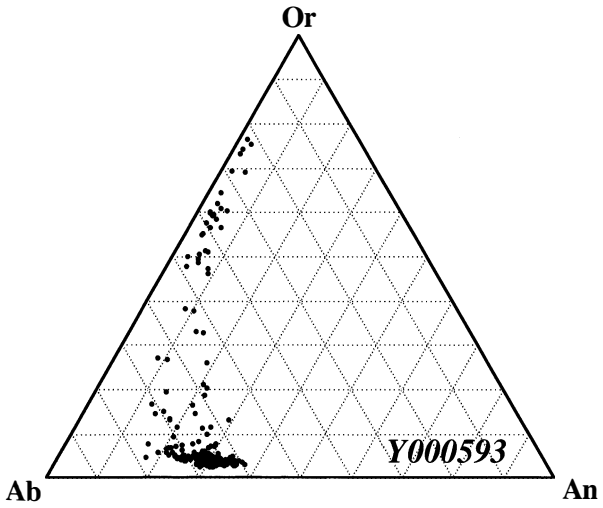


*Fig. 10. Major element compositions (Ca, Na and K) of feldspars in Y000593. Plagioclase has the composition of $An_{35}Ab_{62}Or_3$~ $An_{20}Ab_{74}Or_6$. K-feldspar has a wide range of composition, reaching $Or_{75}$.*

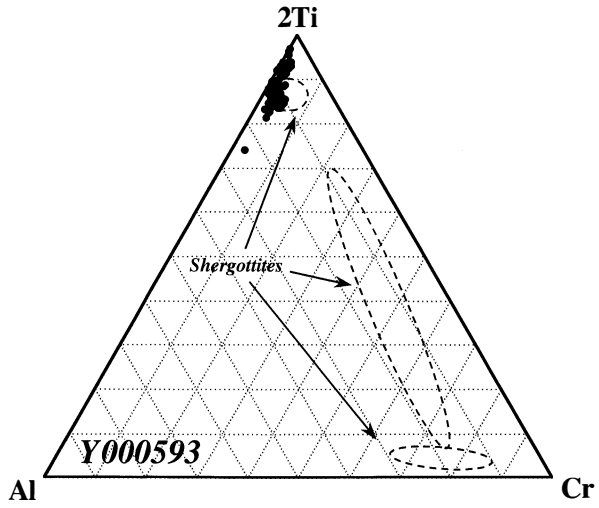


*Fig. 11. Major element compositions (Cr, Al and Ti) of spinels in Y000593. Spinels in Y000593 are Ti-rich magnetite (ulvöspinel). The dashed circles show the compositions of spinels in shergottites, which are quite different from those of Y000593.*

atomic diffusion of olivine relative to pyroxene (*e.g.*, Misener, 1974; Fujino *et al.*, 1990). Because Fe enrichment was observed near the rims adjacent to the mesostasis and the degree of chemical zoning was larger in olivine than pyroxene, chemical zoning would

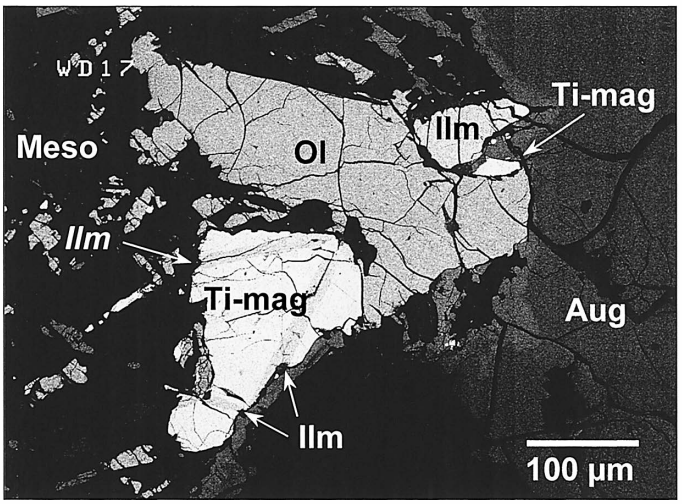


*Fig. 12. BSE image of the mesostasis area including opaque minerals in Y000593. Ti-rich magnetite grain in this image shows ilmenite exsolution lamellae parallel to three orientations (probably parallel to (111)). An individual ilmenite grain is also present. Ti-mag: Ti-rich magnetite. Ilm: ilmenite. Ol: olivine. Aug: augite. Meso: mesostasis.*

be produced by interaction with the Fe-rich intercumulus melt. This scenario has been proposed by Harvey and McSween (1992a) and we believe that this is also applicable for the case of Y000593. Before accumulation of augite and olivine, both minerals would be homogenized. The formation of symplectite exsolution in olivine would also occur at this stage due to relatively slow cooling. The next process included formation of a cumulus network in the magma, producing interstitial melt to both augite and olivine and modifying homogeneous compositions into zoned ones at the rims of augite and olivine. We also suggest that "overgrowth" of low-Ca pyroxene at the extreme edges of cumulus augite occurred at this stage. Feldspar minerals and Ti-rich magnetite crystallized in the intercumulus melt, forming the mesostasis. Our thin sections do not give definite information of the origin of "rust" in olivine and the mesostasis. However, Treiman and Goodrich (2002) reported that at least some of this material is of Martian origin as other nakhlites contain pre-terrestrial alteration products. Imae *et al.* (2002b) analyzed Xe and Kr isotopes of the weathering products and also suggested their Martian origin. Therefore, the final process that affected Y000593 was aqueous alteration on Mars forming "rust" in olivine and the mesostasis.

## 6. Comparisons with other nakhlites

### *6.1. Petrography*

The texture of Y000593 is generally similar to all other nakhlites (*e.g.*, Harvey and McSween 1992a; Lentz *et al.*, 1999; Mikouchi and Miyamoto, 2001; Sautter *et al.*, 2002). All the nakhlites have a similar ratios of modal proportions of augite and olivine (augite/olivine=*ca.* 4~6) (*e.g.*, Lentz *et al.*, 1999; Sautter *et al.*, 2002). The

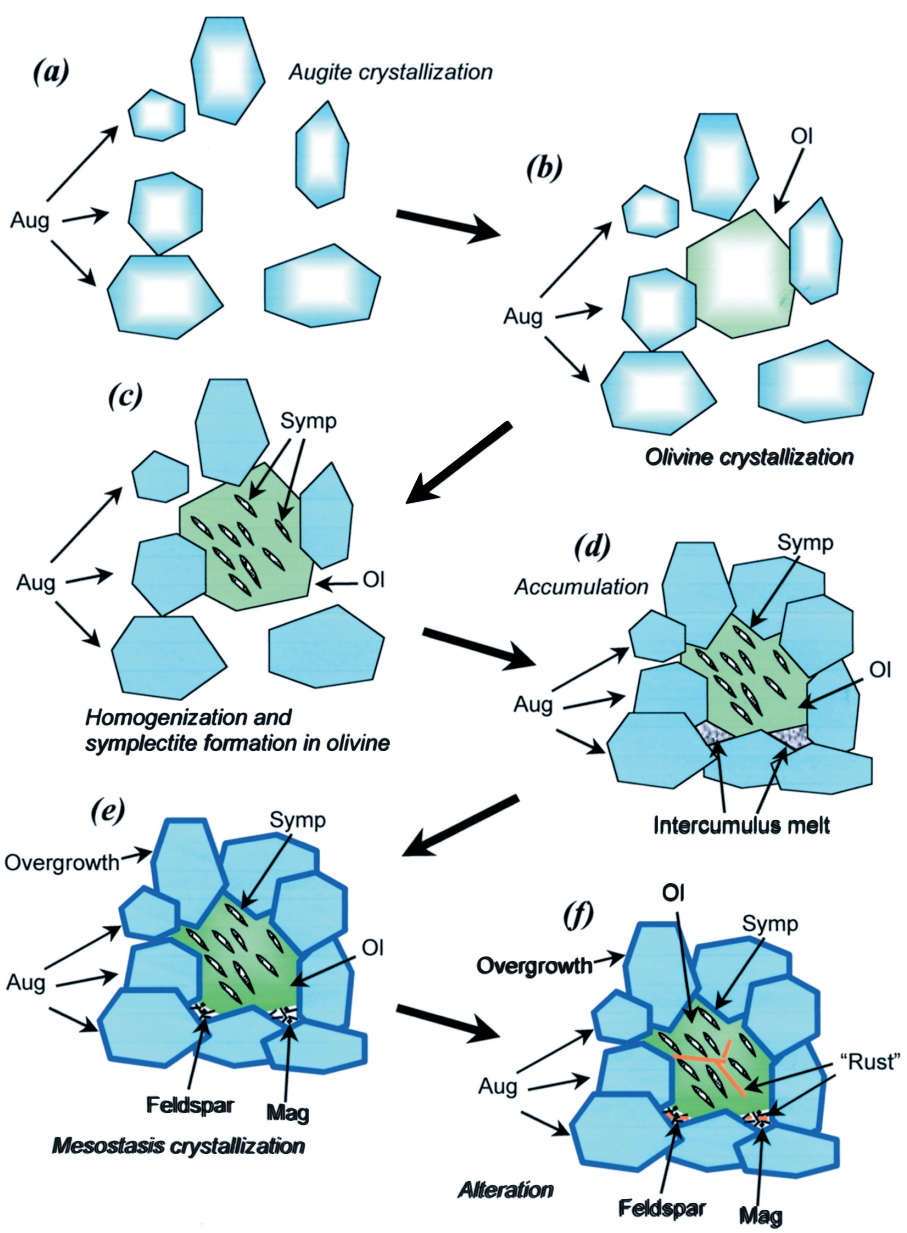


*Fig. 13. Schematic illustration showing the formation history of Y000593. (a) Augite crystallization from a magma. Aug: augite. (b) Olivine crystallization from the same or different magma. Ol: olivine. (c) Homogenization of chemical composition of both augite and olivine. Symplectite formation occurred at this stage. Symp: symplectite. (d) Accumulation of augite and olivine occurred, forming a cumulate network with intercumulus melt. (e) The mesostasis rapidly crystallized and chemical zoning was produced at the rims of augite (not extensive) and olivine adjacent to the mesostasis. "Overgrowth" of Fe-rich pyroxene was also formed. Mag: magnetite. (f) Aqueous alteration affected olivine and the mesostasis, forming brown "rusty" products ("Rust").*

*Table 2. Mesostasis abundance and related mineralogical characteristics of nakhlites.*

| Sample name | Mesostasis abundance | Plagioclase size | Olivine composition at the rim | Pyroxene composition at the rim |
|---|---|---|---|---|
| NWA817 | ~20 vol% | <5 μm wide | $Fa_{85}$ | Atomic Fe/(Mg+Mg) = 0.75 |
| Y000593 | ~10 vol% | ~20 μm wide | $Fa_{82}$ | Atomic Fe/(Mg+Mg) = 0.71 |
| Nakhla | ~5 vol% | ~50 μm wide | $Fa_{72}$ | Atomic Fe/(Mg+Mg) = 0.66 |
| Governador Valadares | ~5 vol% | ~50 μm wide | $Fa_{70}$ | Atomic Fe/(Mg+Mg) = 0.66 |
| Lafayette | ~5 vol% | ~50 μm wide | $Fa_{68}$ | Atomic Fe/(Mg+Mg) = 0.50 |

grain sizes of cumulus augite and olivine in Y000593 are also very similar (average 0.5–1.0 mm long with a maximum of 1.5 mm long) to those of other nakhlites (*e.g.*, Lentz *et al.*, 1999; Sautter *et al.*, 2002). The most notable petrographic difference between Y000593 and other nakhlites is the abundance of the mesostasis (Table 2). NWA817 has similar (or slightly higher) modal abundance of the mesostasis, but the radiating plagioclase is rare (or very thin) in NWA817 (Mikouchi and Miyamoto, 2001; Sautter *et al.*, 2002). The mesostasis in NWA817 is rather composed of Si-rich feldspathic glass with skeletal Ti-rich magnetite, suggesting a faster cooling of the mesostasis (Mikouchi and Miyamoto, 2001; Sautter *et al.*, 2002). The mesostasis mineralogy of Y000593 is rather similar to Nakhla, Governador Valadares and Lafayette with the presence of radiating plagioclase laths. However, plagioclase in Y000593 is thinner (~20 $\mu$m wide) compared to those in Nakhla, Governador Valadares and Lafayette (~50 $\mu$m) (Table 2). Bunch and Reid (1975) and Friedman *et al.* (1998) made similar observations on the plagioclase textures in the nakhlite mesostasis. The different sizes of plagioclase in the mesostasis suggest that the cooling rate of Y000593 was faster than those of other nakhlites, perhaps due to a shallower location in the igneous body (Harvey and McSween, 1992a; Mikouchi and Miyamoto, 2002; Mikouchi *et al.*, 2002). The difference in the mesostasis abundance between Y000593/NWA817 and Nakhla/Governador Valadares/Lafayette suggests that NWA817 and Y000593 formed at locations in a cooling cumulus pile where the abundances of cumulus phases were lower than other nakhlites. The abundance of the mesostasis or the degree of "packing" of cumulus phases may be related to the burial depths of nakhlites (Table 2). The different mesostasis mineralogy also relates to other mineralogical characteristics as discussed in the following chapter and also reported in Imae *et al.* (2002b).

The degree of aqueous alteration of Y000593 is also generally similar to those of other nakhlites (*e.g.*, Treiman *et al.*, 1993). This suggests that fluid activity was uniform throughout the nakhlite igneous body.

### 6.2. *Augite mineralogy*

The chemical composition of the augite core in Y000593 is nearly identical to those of other nakhlites, suggesting that they have a similar petrogenesis (*e.g.*, Harvey and McSween, 1992a; Wadhwa and Crozaz, 1995) (Figs. 3 and 14). However, augite grains in Y000593 have a distinctive rim composition different from any other nakhlite

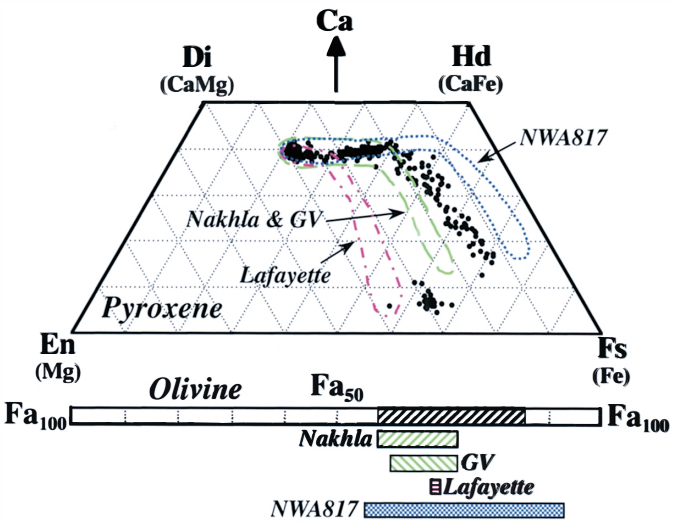


*Fig. 14. Pyroxene quadrilateral of Y000593 along with the pyroxene compositions of Nakhla, Governador Valadares (GV), Lafayette and NWA817. Their olivine compositions (Fa and Fo contents) are also shown. Augite cores of all nakhlites have an identical composition although the rim compositions are different. Olivine compositions of nakhlites have variations in both core and rim compositions.*

pyroxenes (Figs. 3 and 14). Nakhla and Governador Valadares are the most similar in terms of the pyroxene rim compositions. Pyroxenes in Nakhla and Governador Valadares have Fe-rich compositions with variable Wo contents (but constant En) similar to Y000593 due to the presence of fine exsolution lamellae (Mikouchi and Miyamoto, 1998). Nevertheless, the most Fe-rich composition of Y000593 pyroxene is more Fe-rich than those of Nakhla and Governador Valadares. NWA817 does not contain Fe-rich augite with variable Wo content in our sample (Mikouchi and Miyamoto, 2001), but Sautter *et al.* (2002) reported the presence of very Fe-rich pyroxenes with variable Wo content. These Fe-rich pyroxenes are more Fe-rich than that of Y000593 (Fig. 14). Lafayette is quite different from other nakhlites including Y000593 in its homogeneous composition except for the extreme edge adjacent to the mesostasis. This homogeneous composition is probably due to slower cooling. Thus, compositions of Y000593 pyroxenes are intermediate between those of Nakhla/Governador Valadares and NWA817.

### *6.3. Olivine mineralogy*

All the nakhlites including Y000593 have unique olivine compositions (Figs. 3 and 14). Olivine composition is more variable than pyroxene in nakhlites (Fig. 5). This is probably because olivine has faster atomic diffusion rates than those of pyroxene (*e.g.*, Misener, 1974; Fujino *et al.*, 1990) and its composition is sensitive to minor differences in thermal history. The most magnesian composition of Y000593 olivine ($Fa_{58}$) is identical to that of Nakhla, but Y000593 olivine extends to more ferroan compositions ($Fa_{82}$) than Nakhla ($Fa_{78}$). NWA817 olivine also has Fe-rich compositions of $Fa_{\sim 85}$,

but the most magnesian olivine is more Mg-rich ($Fa_{54}$). As is seen in augite composition, Lafayette olivine is almost completely homogeneous ($Fa_{68}$). In this sense, Lafayette appears to have been located at the deepest position in the cooling cumulus pile, causing homogenization of its mineral compositions (*e.g.*, Harvey and McSween, 1992a). The rim compositions of Nakhla and Governador Valadares olivines are very similar ($Fa_{70-72}$) to each other. NWA817 and Y000593 olivines have more Fe-rich olivine rim compositions of $Fa_{92}$ and $Fa_{82}$, respectively (Mikouchi and Miyamoto, 2001). The Fe-rich compositions of NWA817 and Y000593 olivine rims are consistent with high abundances of their mesostases. These data suggest that the mesostasis crystallization of NWA817 and Y000593 occurred very near the Martian surface. Y000593 provides several pieces of evidence (*e.g.*, plagioclase size in the mesostasis, olivine composition) that it was located slightly deeper than NWA817. The final crystallization of Nakhla and Governador Valadares would occur the locations intermediate between those of Y000593 and Lafayette.

Thus, nakhlite olivines are a good indicator of the cooling history of nakhlites. In a previous study, we estimated cooling rates of olivines from Nakhla, Lafayette, Governador Valadares and NWA817 by using chemical zoning of Fe-Mg and Ca at their olivine rims adjacent to the mesostases (Mikouchi and Miyamoto, 2002). We computed the Fa and Ca zoning profiles at various cooling rates from 1100°C to 700°C after we assumed that initial olivine compositions are homogeneous ($Fa_{54}$, CaO: 0.54 wt%). We revised the Fe-Mg diffusion rate of Misener (1974) by dependence of oxygen fugacity and Fe/Mg ratios of olivine (Miyamoto *et al.*, 2002). In this calculation, we set the oxygen fugacity at the QFM buffer that is the estimated redox condition of nakhlites (*e.g.*, Reid and Bunch, 1975). Ca diffusion data are from Jurewicz and Watson (1988). The obtained cooling rates correspond to a burial depth ranging from $\ll$1 m for NWA817 to $>$30 m for Lafayette. Nakhla and Governador Valadares are intermediate between these two (3–10 m). Because Y000593 appears to have been located intermediate between NWA817 and Nakhla/Governador Valadares, the burial depth of Y000593 would be shallower than 3 m from the surface. Olivine may have started cooling from higher temperature than 1100°C. In that case, olivine should have experienced faster cooling rates than the result obtained for the 1100–700°C temperature range. If olivine started cooling from 1000°C, the obtained cooling rates would be about one order of magnitude slower than those from 1100°C. Even if this is the case, the burial depth for NWA817 is shallower than 1 m. Lafayette has the slightly deeper burial depth.

The presence of symplectic inclusions in olivine has previously been observed only in Nakhla and Governador Valadares (Mikouchi and Miyamoto, 1998; Mikouchi *et al.*, 2000). This is consistent with the similarity in olivine compositions between Y000593 and Nakhla/Governador Valadares. The reason for the absence of such symplectites in NWA817 and Lafayette is unclear. Perhaps, relatively fast cooling of the cumulus augite and olivine in NWA817 (corresponding to a~b~c stages of Fig. 13) prevented exsolution of symplectites. Lafayette is distinct from other nakhlites in many respects and it may have a different history from other nakhlites.

### *6.4. Opaque mineralogy*

The chemical composition of Ti-rich magnetite and ilmenite in Y000593 is generally similar to those of other nakhlites, suggesting that all nakhlites formed under similar redox conditions near the QFM buffer (*e.g.*, Reid and Bunch, 1975). We have not performed a detailed analysis on sulfides, but the presence of pyrite has been reported from other nakhlites (*e.g.*, Bunch and Reid, 1975).

## 7. Conclusions

There is no doubt that Y000593 is a new nakhlite (not paired with any other previously known nakhlites) since it was found in Antarctica, thousands of kilometers away from other nakhlites. These rocks, including Y000593, share similar mineralogy and ages, suggesting that they came from the same igneous body on Mars and were ejected by the same impact event (*e.g.*, Bogard *et al.*, 1984; Bogard, 1995; Bunch and Reid, 1975; Eugster *et al.*, 1997; Harvey and McSween, 1992a; Marty *et al.*, 2001; Imae *et al.*, 2002a, b; Lentz *et al.*, 1999; Mikouchi and Miyamoto, 1998, 2002; Mikouchi *et al.*, 2002; Nakamura *et al.*, 1982, 2002; Okazaki *et al.*, 2002; Oura *et al.*, 2002; Reid and Bunch, 1975; Sautter *et al.*, 2002; Shih *et al.*, 1996, 1998, 2002; Ueda *et al.*, 2002; Wadhwa and Crozaz, 1995; Yamashita *et al.*, 2002). In other words, it is very notable that we have nakhlite samples from a variety of terrestrial locations that show slightly different mineralogy from each other. The difference might be due to different thermal histories due to different locations (burial depths) in the same cooling cumulate pile (*e.g.*, Harvey and McSween, 1992a; Imae *et al.*, 2002b; Lentz *et al.*, 1999; Mikouchi and Miyamoto, 1998, 2002; Mikouchi *et al.*, 2002; Wadhwa and Crozaz, 1995). Y000593 is most similar to Nakhla and the formation of cumulus phases occurs under the same conditions (Fig. 13). The similarity between Y000593 and Nakhla is also found in reflectance spectra (Ueda *et al.*, 2002). Later mesostasis crystallization of Y000593 was more rapid than Nakhla due to its faster cooling rate, and produced minor differences between them. We previously estimated that the burial depths of Nakhla and NWA817 were 4–5 m and 0.5 m, respectively, according to the Fa zoning profiles of olivine (Mikouchi and Miyamoto, 2002). This study suggests that Y000593 would be located between NWA817 and Nakhla. The abundance of the mesostasis or the degree of "packing" of cumulus phases may be related to the burial depths of nakhlites (Imae *et al.*, 2002b).

## Acknowledgments

The Y000593 samples were kindly allocated by NIPR as a part of the consortium study. We thank Drs. N. Imae, K. Misawa, and H. Kojima for useful discussions and Drs. P.C. Buchanan and R.C.F. Lentz for their constructive reviews of the manuscript. We are indebted to Mr. O. Tachikawa and Mr. H. Yoshida for their technical assistance during electron beam analyses. The electron microscopy was performed in the Electron Microbeam Analysis Facility for mineralogy at Department of Earth and Planetary Science, University of Tokyo.

## References

Bogard, D.D. (1995): Exposure-age-initiating events for Martian meteorites: Three or four? Lunar and Planetary Science XXVI. Houston, Lunar Planet. Inst., 143–144.

Bogard, D.D., Nyquist, L.E. and Johnson, P. (1984): Noble gas contents of shergottites and implications for the Martian origin of SNC meteorites. Geochim. Cosmochim. Acta, **48**, 1723–1739.

Bunch, T.E. and Reid, A.M. (1975): The nakhlites I: Petrography and mineral chemistry. Meteoritics, **10**, 303–315.

Eugster, O., Weigel, A. and Polnau, E. (1997): Ejection times of Martian meteorites. Geochim. Cosmochim. Acta, **61**, 2749–2757.

Friedman, R.C., Taylor, G.J. and Treiman, A.H. (1998): Nakhlites and Theo's flow: Formation of extrusive pyroxenites. Lunar and Planetary Science XXIX. Houston, Lunar Planet. Inst., Abstract #1190 (CD-ROM).

Fujino, K., Naohara, H. and Momoi, H. (1990): Direct determination of cation diffusion coefficients in pyroxene. EOS, **71**, 943.

Harvey, R.P. and McSween, H.Y., Jr. (1992a): Petrogenesis of the nakhlite meteorites - Evidence from cumulate mineral zoning. Geochim. Cosmochim. Acta, **56**, 1655–1663.

Harvey, R.P. and McSween, H.Y., Jr. (1992b): The parent magma of the nakhlite meteorites: Clues from melt inclusions. Earth Planet. Sci. Lett., **111**, 467–482.

Imae, N., Okazaki, R., Kojima, H. and Nagao, K (2002a): The first nakhlite from Antarctica. Lunar and Planetary Science XXXIII. Houston, Lunar Planet. Inst., Abstract #1483 (CD-ROM).

Imae, N., Ikeda, Y., Shinoda, K., Kojima, H. and Iwata, N. (2002b): Two nakhlites from Antarctica: Y 000593 and Y000749. Antarctic Meteorites XXVII. Tokyo, Natl Inst. Polar Res., 45–47.

Imae, N., Iwata, N. and Shimoda, Y. (2002c): Search for Antarctic meteorites in the bare ice field around the Yamato Mountains by JARE-41. Antarct. Meteorite Res., **15**, 1–24.

Irving, A.J., Kuehner, S.M., Rumble, D. III, Carlson, R.W., Hupé, A.C. and Hupé, G.M. (2002): Petrology and isotopic composition of orthopyroxene-bearing nakhlite NWA 998. Meteorit. Planet. Sci., **37**, A70.

Jurewicz, A.J.G. and Watson, E.B. (1988): Cations in olivine, part 2: Diffusion in olivine xenocrysts, with application to petrology and mineral physics. Contrib. Mineral. Petrol., **99**, 186–201.

Kojima, H. and Imae, N., ed. (2001): Meteorite Newsletter, **10**, (2), 9 p.

Kojima, H., Nakamura, N., Imae, N. and Misawa, K. (2002): The Yamato nakhlite consortium. Antarctic Meteorites XXVII. Tokyo, Natl Inst. Polar Res., 66–68.

Lentz, R.C.F., Taylor, G.J. and Treiman, A.H. (1999): Formation of a martian pyroxenite: A comparative study of the nakhlite meteorites and Theo's Flow. Meteorit. Planet. Sci., **34**, 919–932.

Marty, B., Marti, K. and the Theodore Monod Consortium (2001): Noble gases in new SNC meteorites NWA 817 and NWA 480. Meteorit. Planet. Sci., **36**, A122–A123.

McSween, H.Y., Jr. (1994): What we have learned about Mars from SNC meteorites. Meteoritics, **29**, 757–779.

Meyer, C. (1998): Mars Meteorite Compendium—2001. Houston, NASA Johnson Space Center 237 p. (http://www/curator.jsc.nasa.gov/curator/antmet/mmc/mmc.htm).

Mikouchi, T. and Miyamoto, M. (1998): Pyroxene and olivine microstructures in nakhlite Martian meteorites: Implication for their thermal history. Lunar and Planetary Science XXIX. Houston, Lunar Planet. Inst., Abstract #1574 (CD-ROM).

Mikouchi, T. and Miyamoto, M. (2001): Northwest Africa 817: A new nakhlite similar to others but distinct. Meteorit. Planet. Sci., **36**, A134.

Mikouchi, T. and Miyamoto, M. (2002): Comparative cooling rates of nakhlites as inferred from iron-magnesium and calcium zoning of olivines. Lunar and Planetary Science XXXIII. Houston, Lunar Planet. Inst., Abstract #1343 (CD-ROM).

Mikouchi, T., Yamada, I. and Miyamoto, M. (2000): Symplectic exsolution in olivine from the Nakhla martian meteorite. Meteorit. Planet. Sci., **35**, 937–942.

Mikouchi, T., Koizumi, E., Monkawa, A., Ueda, Y. and Miyamoto, M. (2002): Comparative mineralogy of the new nakhlite Yamato 000593 with other nakhlite Martian meteorites. Antarctic Meteorites

XXVII. Tokyo, Natl Inst. Polar Res., 83–85.
Misener, D.J. (1974): Cation diffusion in olivine to 1400℃ and 35 kbar. Geochemical Transport and Kinetics, ed. by A.W. Hoffmann *et al.* Washington D.C., Carnegie Inst. of Washington, 117–129.
Miyamoto, M., Mikouchi, T. and Arai, T. (2002) Comparison of Fe-Mg interdiffusion coefficients in olivine. Antarct. Meteorite Res., **15**, 143–151.
Nakamura, N., Unruh, D.M., Tatsumoto, M. and Hutchison, R. (1982): Origin and evolution of the Nakhla meteorite inferred from the Sm-Nd and U-Pb systematics and REE, Ba, Sr, Rb and K abundances. Geochim. Cosmochim. Acta, **46**, 1555–1573.
Nakamura, N., Yamakawa, A., Yamashita, K., Kobayashi, T., Imae, N., Misawa, K. and Kojima, H. (2002): REE abundances and Rb-Sr age of a new Antarctic nakhlite Yamato 000593. Antarctic Meteorites XXVII. Tokyo, Natl Inst. Polar Res., 112–114.
Okazaki, R., Nagao, K., Imae, N. and Kojima, H. (2002): Noble gases in Antarctic nakhlites, Yamato 000593 and Yamato 000749. Antarctic Meteorites XXVII. Tokyo, Natl Inst. Polar Res., 134–136.
Oura, Y., Shirai, N. and Ebihara, M. (2002): Chemical composition of Y000593 and Y000749. Antarctic Meteorites XXVII. Tokyo, Natl Inst. Polar Res., 143–145.
Reid, A.M. and Bunch, T.E. (1975): The nakhlites part II: Where, when and how. Meteoritics, **10**, 317–324.
Sautter, V., Barrat, J.A., Jambon, A., Lorand, J.P., Gillet, Ph. and Javoy, M. (2002): A new Martian meteorite from Morocco: the nakhlite North West Africa 817. Earth Planet. Sci. Lett., **195**, 223–238.
Shih, C.-Y., Nyquist, L.E. and Wiesmann, H. (1996): Sm-Nd systematics of nakhlite Governador Valadares. Lunar and Planetary Science XXVII. Houston, Lunar Planet. Inst., 1197–1198.
Shih, C.-Y., Nyquist, L.E., Reese, Y. and Wiesmann, H. (1998): The chronology of the nakhlite, Lafayette: Rb-Sr and Sm-Nd isotopic ages. Lunar and Planetary Science XXIX. Houston, Lunar Planet. Inst., Abstract #1145 (CD-ROM).
Shih, C.-Y., Wiesmann, H., Nyquist, L.E. and Misawa, K. (2002): Crystallization age of Antarctic nakhlite Y000593: Further evidence of nakhlite launch pairing. Antarctic Meteorites XXVII. Tokyo, Natl Inst. Polar Res., 151–153.
Treiman, A.H. and Goodrich, C.A. (2002): Pre-terrestrial aqueous alteration of the Y-000749 nakhlite meteorite. Antarctic Meteorites XXVII. Tokyo, Natl Inst. Polar Res., 166–167.
Treiman, A.H., Barrett, R.A. and Gooding, J.L. (1993): Preterrestrial aqueous alteration of the Lafayette (SNC) meteorite. Meteoritics, **28**, 86–97.
Ueda, Y., Mikouchi, T., Miyamoto, M. and Hiroi, T. (2002): First analysis of the reflectance spectrum of Yamato 000593: The spectroscopic similarity between Yamato 000593 and Nakhla. Antarctic Meteorites XXVII. Tokyo, Natl Inst. Polar Res., 171–173.
Wadhwa, M. and Crozaz, G. (1995): Trace and minor elements in minerals of nakhlites and Chassigny: Clues to their petrogenesis. Geochim. Cosmochim. Acta, **59**, 3629–3645.
Yamashita, K., Nakamura, N., Imae, N., Misawa, K. and Kojima, H. (2002): Pb isotopic signature of Martian meteorite Yamato 000593 (A preliminary report). Antarctic Meteorites XXVII. Tokyo, Natl Inst. Polar Res., 180–182.

*(Received November 13, 2002; Revised manuscript accepted February 3, 2003)*